Article

Modelling Initial Imperfections using Scaled Buckling Modes: A Strain Energy and Entropy Approach

Zdeněk Kala *

Posted Date: 14 November 2023

doi: 10.20944/preprints202311.0862.v1

Keywords: strain energy; entropy; buckling; structural mechanics; structural engineering; steel structures; initial imperfections

Article

Modelling Initial Imperfections Using Scaled Buckling Modes: A Strain Energy and Entropy Approach

Zdeněk Kala

Institute of Structural Mechanics, Faculty of Civil Engineering, Brno University of Technology, 602 00 Brno, Czech Republic; kala.z@fce.vutbr.cz

Abstract: A new utilization of entropy in the context of buckling is presented. The novel concept connecting strain energy and entropy for a pin-ended strut is derived. This concept rationalizes the ranking of buckling modes based on strain energy under the assumption of given entropy. By assigning identical entropy to all buckling modes, they can be ranked according to their deformation energy. Conversely, with identical strain energy assigned to all modes, ranking according to entropy is possible. Decreasing entropy was found to represent the scaling factors of buckling modes that coincide with the measurement of initial out-of-straightness imperfections in IPE160 beams. Applied to steel plane frames, scaled buckling modes can be used to model initial imperfections. It is demonstrated that the entropy (scale factor) for given energy roughly decreases with the inverse square of the mode index. For practical engineering, the study presents the possibility of using scaled buckling modes of steel plane frames to model initial geometric imperfections. Entropy proves to be a valuable complement to strain energy in structural mechanics.

Keywords: strain energy; entropy; buckling; structural mechanics; structural engineering; steel structures; initial imperfections

1. Introduction

The investigation of buckling modes is of great importance in the field of structural engineering and structural mechanics. Understanding the stability behaviour of structures under various loads and conditions is essential to ensuring their safety and reliability [1,2].

Throughout history, the study of structural stability has been intertwined with the evolution of engineering and mathematics [3]. The concept of buckling, where slender columns or beams, which are subjected to axial loads, deform and potentially fail under compression, has captured the attention of engineers and mathematicians for centuries [4]. The history of buckling analysis can be traced back to the 18th century in the works of Euler, who has made significant contributions to the understanding of the stability of columns [5].

As theory advances, so does the capability to investigate the structural behaviour of frame structures [6,7]. The emergence of computer-based analysis and numerical methods have enabled engineers to explore the intricacies of buckling modes in various configurations. A significant advancement has been the introduction of finite element methods and geometrically and materially non-linear solutions [8], capable of analysing the load-bearing capacity of structures with initial imperfections; see, e.g., [9–11].

Currently, the design of structural steel employs a systematic design approach known as the Direct Design Method [12], which explicitly accounts for material and geometric nonlinearities, residual stresses, and the presence of initial imperfections. The shape of these initial imperfections should be defined to take into account their influence on the load-carrying capacity while respecting real-world measures from experiments; see, e.g., [13–15]. Typically, the first buckling mode shape is used to represent these initial imperfections, assuming it to be the most critical [16,17]. However, in cases where the critical buckling loads of two distinct buckling modes coincide, the sensitivity to

 doi:10.20944/preprints202311.0862.v1

imperfections increases significantly [18,19]. In these cases, the buckling mode shapes may be more important than the magnitude of the critical force when modelling initial imperfections.

This article is based on the heuristic argument that if two distinct buckling modes coincide, the system tends to follow the buckling mode with lower energy and higher entropy. Since the entropy of the buckling mode has not yet been studied, a concept of a surrogate model is proposed based on thermodynamics, where entropy naturally occurs.

Thus, a new concept of entropy and virtual temperature based on the equivalence of strain and heat energy in the surrogate model is introduced. The surrogate model is based on an unconventional connection of classical theories: entropy [20], heat energy [20], strain energy [21], and buckling [1]. The entropy is presented as a new indicator of stability and resistance to buckling. The research progresses from a simple beam to more complex structures, such as steel plane frames.

2. State of the Art

The principle of minimum total energy is a fundamental concept in structural mechanics, which is used to determine equilibrium conditions and the behaviour of structural systems [22–26]. In statics of structures, the total energy is composed of the strain energy and the potential energy of the applied static loads. The basic idea is that the structure tends to find a deformation that minimizes the total energy.

Strain energy has been used to calculate the elastic lateral stiffness in frame members [27], to investigate the low yield strain steel energy dissipater [28], to optimize the seismic performance of modular prefabricated four-side connected composite shear walls [29], to model the damage and failure of quasibrittle structures [30], to analyse the effects of aftershocks on structural stability [31], to calculate the elastic global buckling stress of box-shape cold-formed steel built-up columns [32], to achieve an optimized unstiffened steel plate shear wall configuration [33], to study rock deformation [34,35], to evaluate the structural damage of reinforced concrete members [36], to analyse the lateral torsional buckling of corrugated steel web girders [37], to analyse the lateral-torsional buckling of I-beams [38], to analyse the extreme properties of the structural strain energy using eigenvalues problem [39], to analyse the plastic buckling of stainless steel circular cylindrical shells [40], to study the mechanical properties of fiber-reinforced lime-cement concrete [41], to predict the cumulative strain energy of isolators and dampers for seismic design [42], to study the buckling problems of structures with single delamination [43], to analyse the buckling behaviour of carbon nanotubes [44], to study the cyclic hardening-softening characteristics of duplex stainless steel [45], to analyse the shear stress distribution in corrugated steel web bridges [46], to perform elasto-plastic analysis of prestressed reinforced concrete beams [47], to examine the nonlinear buckling behaviour of porous linings reinforced with graphene platelets [48], to investigate the cyclic behaviour of titanium-clad bimetallic steel under large-magnitude cyclic strains [49], to study of limit states of bar structures [50], to analyse the bifurcations points of von Mises trusses [51], to compare the pre-failure and post-failure structural strain energy in order to reflect the structural robustness [52], to study steel columns in fire using a concept based on voxels [53], to derive the stiffness matrix of tapered members with warping and Wagner effects [54], to investigate the elastic buckling behaviour of oblate hemi-ellipsoidal shells under the influence of hydrostatic pressure [55], to study the wind flow loading scenarios of modular steel constructions [56], to develop an accurate model for lateral-torsional buckling analysis and the prediction of inelastic behaviour [57], to study the mechanical properties of rocks under different moisture content [58], to analyze the strain in the concrete and reinforcement within the context of the bending performance [59], to study the plastic buckling of cylindrical oil storage tanks [60], to introduce a novel approach to derive the total potential energy equations of steel members [61], to assess the safety and predict the stability of fractured rocks [62], to study the behaviour of reinforced concrete beams strengthened with externally bonded fiber reinforced polymer materials [63].

Entropy is a term that originated from thermodynamics [64] and informatics [20], but has many applications in other scientific fields, including civil engineering and structural mechanics. Examples of the application of entropy in these fields include: the assessment of the evolution and abrupt changes in water use structure in China [65], structural engineering, water management and urban

Preprints (www.preprints.org) | NOT PEER-REVIEWED | Posted: 14 November 2023 doi:10.20944/preprints202311.0862.v1

modelling [66], structural uncertainties in global response prediction in seismic hazard mitigation [67], decision-making models for selecting subcontractors of large construction companies [68], investigation of mechanical properties of polyurethane porous mixtures [69], seismic performance of underground large-scale frame structures [70], toolbox design for calculating geological entropy in heterogeneous systems [71], signal analysis for assessing wind speed in wind tunnel testing of long span bridges [72], optimization of the performance of tuned mass dampers in reducing seismic responses in tall buildings [73], characterization of the degree of disorder and accumulation of rock microcracks [74], durability of concrete structures affected by environmental conditions [75], development of a dynamic risk control system for sleeve grouting in prefabricated constructions [76], identification of unbalanced bidding using a multi-criteria decision-making approach [77], investigation of the presence of undeclared leader-follower structures in pedestrian evacuation scenarios [78], reliability analysis of a Tibetan timber frame using entropy-based sensitivity analysis [79], construction safety risks in prefabricated subway stations in China [80], assessment of the reliability of steel civil engineering structures exposed to fire temperatures [81], reliability assessment of structural systems [82], damage assessment of civil structures and infrastructures based on entropy measurements [83], modelling of hot flow behaviour and grain evolution of alloys [84], assessment of asphalt mixture uniformity with consideration to the characteristics of particles [85], establishment of attribute weights in multi-criteria decision-making [86], global sensitivity analysis of reliability [87], categorization of buckling modes in steel plane frames [88]. Shannon's entropy was used as a measure of the uniformity or orderliness of examined data spectrum in articles [66,71,74,83,85,88].

In civil engineering, the topic of buckling is much more attractive than the topic of entropy, see Figure 1. On the topic of buckling 17898 articles have been published in the category of Civil Engineering, 16167 articles in the category of Mechanics and 7783 articles in the category of Construction Building Technology. On the topic of entropy 2199 articles have been published in the category of Civil Engineering, 8459 articles in the category of Mechanics and 662 articles in the category of Construction Building Technology. Entropy is most attractive in the Materials Science Multidisciplinary category, where a total of 28710 articles have been published. In total, 277728 articles were published on entropy, while only 64808 were published on buckling. The data was obtained from the Web of Science database on November 12th, 2023.

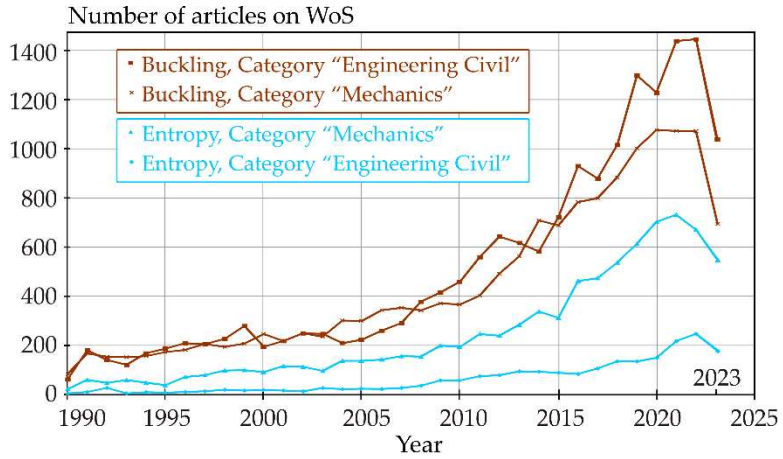

Figure 1. Number of publications in "Civil engineering" and "Mechanics" Web of Science categories (Web of Science core collection database, 12 November 2023), topic "buckling" and "entropy".

3. Buckling of a Pin-ended Strut

Consider a slender strut with pin-ended supports subjected to an axial compressive load P. The strut remains ideally straight until the load reaches its critical value P_{cr} and buckling occurs [1,2]. The critical load places the strut in a state of unstable equilibrium, where, in addition to equilibrium on the straight beam, there also exists equilibrium on the deflected beam, see Figure 2.

Preprints (www.preprints.org) | NOT PEER-REVIEWED | Posted: 14 November 2023 doi:10.20944/preprints202311.0862.v1

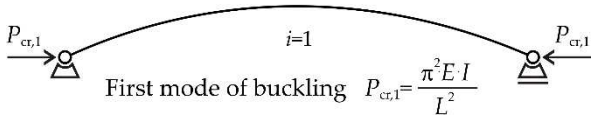

Figure 2. The flexural buckling of the pin-ended strut.

For a strut under critical load, bending deformation can be described according to the Euler–Bernoulli beam theory using the differential equation:

$$\frac{dy^2(x)}{dx^2}+\frac{P}{E\cdot I}y=0\,, \tag{1}$$

where $y(x)$ is the lateral deflection, E is Young's modulus, and I is the second moment of area. This equation is a linear, nonhomogeneous differential equation of the second order with constant coefficients. Upon substituting $\alpha^2 = P/(E{\cdot}I)$, the particular solution of the differential equation can be expressed in the form:

$$y(x)=c_1\cdot\sin(\alpha\cdot x)+c_2\cdot\cos(\alpha\cdot x)\,,\ \text{for}\ \ x\in[0,\,L]\,. \tag{2}$$

From the boundary conditions, it can be calculated that c_2=0 for $y(0)$=0 and $c_1{\cdot}\sin(\alpha{\cdot}L)$=0 for $y(L)$=0, where L is the strut length and c_1 is indeterminate amplitude. By using c_1>0, it can be obtained that $\sin(\alpha{\cdot}L)$=0, and thus $\alpha = i^*\pi/L$, where i represents a natural number of the buckling mode. The corresponding buckling modes can be derived from Equation (2) as eigenmodes, resulting in deformation patterns that are characterized by sine functions.

$$y(x)=c_1\cdot\sin\left(i\frac{\pi\cdot x}{L}\right),\ \text{for}\ \ x\in[0,\,L]\,,\ i=1,\,2,\,..\,, \tag{3}$$

where i is the number of half-sine curvatures that occur lengthwise. Buckling modes can be described as the shapes the strut assumes during buckling, with the sine function playing a crucial role in their formulation, see Figure 3.

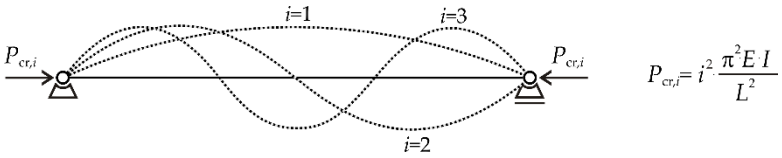

Figure 3. The buckling modes of the pin-ended strut.

Using the previously defined equation $\alpha^2 = P/(E{\cdot}I)$, the critical loads are:

$$P_{cr,i}=i^2\cdot\pi^2\frac{E\cdot I}{L^2},\ \text{for}\ i=1,\,2,\,..\,, \tag{4}$$

Equation (4) provides the standard critical load at which buckling occurs in a pin-ended strut. This provides insight into the behaviour of slender struts under axial compression, and valuable understanding of the design and analysis of structural systems.

3.1. Strain Energy

The discretization of $y(x)$ is performed at the centroids of finite elements. By introducing $(j\text{-}0.5)/N$ instead of x/L, Equation (3) can be rewritten in the discrete form:

$$f_{ij}=c_1\cdot\sin\left(i\frac{\pi\cdot(j-0.5)}{N}\right),\ \text{for}\ j=0,\,1,\,\ldots N, \tag{5}$$

where j = 1, 2, .. N and N is the number of beam elements. The elements are considered to have the same length. In differential form, the total internal potential energy (strain energy) of the i-th buckling mode can be obtained as:

Preprints (www.preprints.org) | NOT PEER-REVIEWED | Posted: 14 November 2023 doi:10.20944/preprints202311.0862.v1

$$\Delta\Pi_i = \frac{1}{2}\int_0^L E\cdot I\left(\frac{dy^2(x)}{dx^2}\right)^2 dx = \frac{1}{2}\int_0^L E\cdot I\left(c_1\cdot\left(i\frac{\pi}{L}\right)^2\cdot\sin\left(i\frac{\pi\cdot x}{L}\right)\right)^2 dx = i^4\cdot E\cdot I\cdot\frac{c_1^2\cdot\pi^4}{4\cdot L^3}. \quad (6)$$

The value of $\Delta\Pi_i$ represents the difference between the zero-strain energy of the unloaded beam and the strain energy of the buckled beam.

It can be noted that the square of the second derivative can be replaced by the product of the function value and the fourth derivative, $E\cdot I\cdot(y'')^2 = y\cdot E\cdot I\cdot y''''$. In this expression, the term involving the fourth derivative, $E\cdot I\cdot y''''$, represents a fictitious transverse load action.

According to the principle of conservation of mechanical energy, strain energy from internal forces $\Delta\Pi_i$ (from bending moment) is equal to the potential energy of external forces $\Delta\Pi_e$ (from load action $P_{cr,i}$).

$$\Delta\Pi_e = \frac{1}{2}\cdot P_{cr,i}\cdot\int_0^L\left(\frac{dy(x)}{dx}\right)^2 dx = \frac{1}{2}\cdot i^2\cdot\pi^2\frac{E\cdot I}{L^2}\cdot\int_0^L\left(c_1\cdot i\frac{\pi}{L}\cdot\cos\left(i\frac{\pi\cdot x}{L}\right)\right)^2 dx = i^4\cdot E\cdot I\cdot\frac{c_1^2\cdot\pi^4}{4\cdot L^3}. \quad (7)$$

The discrete form of Equation (6) is used to introduce discrete entropy. By introducing L/N instead of dx and j/N instead of x/L, Equation (6) can be rewritten in the discrete form as:

$$\Delta\Pi_i = \sum_{j=1}^{N}\Delta\Pi_{ij} = \frac{1}{2}\sum_{j=1}^{N}E\cdot I\cdot\left(c_1\cdot\left(i\frac{\pi}{L}\right)^2\cdot\sin\left(i\frac{\pi\cdot(j-0.5)}{N}\right)\right)^2\frac{L}{N}, \text{ for } N > i. \quad (8)$$

when $N > i$ and i is the index of buckling mode. The discrete form is suitable both for use in the finite element method and in connection with entropy. One member of the series $\Delta\Pi_{ij}$ is the strain energy of a single element of the strut. The square of the sine function in Equation (8) converges to the value of $N/2$.

$$\sum_{j=1}^{N}\left(\sin\left(i\frac{\pi\cdot(j-0.5)}{N}\right)\right)^2 = \frac{N}{2}, \text{ for } N > i. \quad (9)$$

Let each buckling mode have its own scale factor using amplitude c_i. By substituting Equation (9) into Equation (8), the sum of discrete strain energy is equal to the value calculated from Equation (6).

$$\Delta\Pi_i = i^4\cdot E\cdot I\cdot\frac{c_i^2\cdot\pi^4}{4\cdot L^3}, \quad (10)$$

where i is the buckling mode number, E is the elastic Young's modulus, I is the second moment of area, L is the length of the specimen and c_i is the amplitude of the half-sine curvature that occurs lengthwise.

3.2. Why Entropy?

In thermodynamics, any equilibrium state can be characterized either as a state of maximum entropy for a given energy or as a state of minimum energy for a given entropy [89]. In structural mechanics, the principle of minimum total potential energy exists [90], but the principle of maximum entropy is not commonly considered.

In structural mechanics, the total potential energy is the sum of the strain energy stored in a deformed structure and the potential energy associated with load action. Structural mechanics uses the fundamental principles of Lagrangian mechanics. In the case of static loading, the structure is in equilibrium when its total potential energy is minimized.

In Euler buckling, the rank of buckling modes is determined by the ranking from the smallest critical force to the largest. This is the most common approach for ranking buckling modes, with the first one considered the most dangerous [91]. Ranking based on the total potential energy is not possible without solving the indeterminate deformation because the total energy is a function of the indeterminate amplitude c_i, as seen, for example, in Equation (10). However, if it is possible to link

Preprints (www.preprints.org) | NOT PEER-REVIEWED | Posted: 14 November 2023 doi:10.20944/preprints202311.0862.v1

energy with entropy, ranking based on the total potential energy is justified. It is sufficient to perform the analysis solely based on strain energy since the potential energy of the load action has the same value.

If it is possible to decompose strain energy using entropy, then ranking of buckling modes based on energy will be possible. By assigning the same entropy to all buckling modes, buckling modes can be ranked by strain energy (from the smallest to the largest). Analogously, when the same strain energy is assigned to all buckling modes, buckling modes can be ranked by entropy from the largest to the smallest. It can be expected that the first in the ranking will be the buckling mode with the lowest critical force, and that ranking by critical forces will be the same or very similar to the ascending ranking by strain energy or the descending ranking by entropy. A new perspective is introduced by considering entropy, justifying the ranking of buckling modes based on strain energy.

Structural mechanics uses the energies in the system following the fundamental principles of Lagrangian mechanics but does not consider entropy. The question is how to calculate entropy for a deformed structure. One of the approaches may involve a surrogate model based on thermodynamics and an isothermal process in gases.

Entropy can be viewed as a characteristic closely related to energy [64,92]. In thermodynamics, the heat energy is generated as a result of changes in the entropy of the system [20]. In modern theories, the entropy can be described using the relationship based on the energy balance [93].

$$F \cdot \Delta x = T \cdot \Delta S \,. \tag{11}$$

Equation (11) relates mechanical work to the thermodynamic work. The left-hand side of the equation is the mechanical work performed by force F on path Δx as the body moves. The right-hand side of Equation (11) is the heat energy produced by the system at temperature T due to changes in the entropy of the system ΔS; see, e.g., [20]. Temperature can be understood as the statistical weight by which energy is assessed in terms of entropy [92].

3.3. Entropy in the Surrogate model

Let us consider a surrogate model where the strain energy of the deformed structure can be decomposed into temperature and entropy. For this purpose, the strain energy is transformed into gas energy. Since we are investigating the characteristics of a surrogate model, the terms entropy ΔS_i and virtual temperature T_i are used. Following Equation (11), we can write:

$$\Delta \Pi_i = T_i \cdot \Delta S_i \,, \tag{12}$$

where $\Delta \Pi_i$ is the strain energy of the buckled strut from the previous chapter, and the right-hand side is heat energy associated with a gas surrogate model from the following chapter.

When virtual temperature T_i is constant, the change in entropy ΔS can be expressed as the work of an ideal gas with constant mass m during an isothermal process. Under constant T_i, the internal energy of the gas remains unchanged. Thus, the heat absorbed during pressure change equals the work done by the gas; see, e.g., [94]. The entire system is isolated, meaning there is no exchange of particles or energy with the surrounding environment, i.e., the number of particles and energy remain constant.

The change in entropy of an isothermal process for gases, where pressure varies as a function of volume, can be expressed as:

$$\Delta S = \frac{m \cdot R}{M_m} \ln \frac{\rho_1}{\rho_2} = \frac{m \cdot R}{M_m} \ln \frac{V_2}{V_1} \,, \tag{13}$$

where ρ_1 is the initial pressure, ρ_2 is the final pressure, V_1 is the initial volume, V_2 is the final volume, M_m is the molar mass of the gas and $R = 8.314$ Jmol^{-1}K^{-1} is the molar gas constant; see, e.g., [95].

The change in entropy will be described using volume change. Let us assume that buckling causes gas compression (volume reduction) on the deflection side and expansion (volume increase) on the opposite side of the beam; see Figure 4. The pistons are located at the centroids of the finite elements in the direction of deformation, and the mesh of the finite elements is uniform.

Preprints (www.preprints.org) | NOT PEER-REVIEWED | Posted: 14 November 2023 doi:10.20944/preprints202311.0862.v1

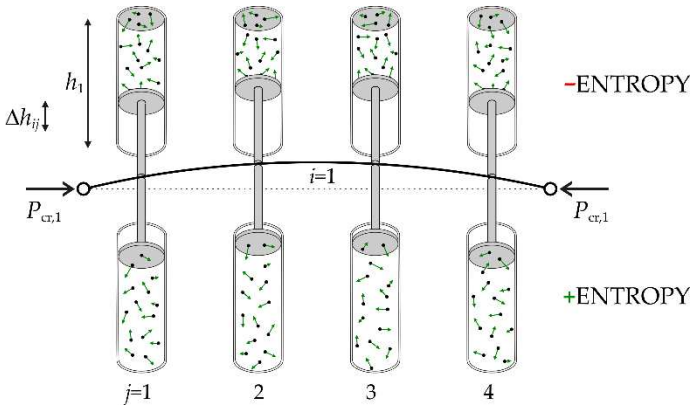

Figure 4. Surrogate model for the transformation buckling mode into entropy.

The change in entropy ΔS_{ij} can be written on the basis of Equation (13). The gas loading the j-th element (compression and expansion) has a mass of m/N, where N is the number of beam elements. The mass of gas in one piston is $0.5 \cdot m/N$. For the j-th element, the equation for the change in entropy on one side of the beam (compression or expansion) can be obtained as:

$$\Delta \bar{S}_{ij} = \frac{m \cdot R}{2 \cdot N \cdot M_m} \ln \frac{V_{ij}}{V_1} = \frac{m \cdot R}{2 \cdot N \cdot M_m} \ln \frac{A \cdot h_{ij}}{A \cdot h_1} = \frac{m \cdot R}{2 \cdot N \cdot M_m} \ln \frac{h_{ij}}{h_1}, \tag{14}$$

where V_{ij} is the final gas volume and h_{ij} je final piston height. The volume V is expressed as the product of the area A and the height h. The change in volume can be expressed as the change in the height h_1 of the piston in the gas vessel, where h_1 is a constant.

Although the link is not direct, the surrogate model converts element deformation into entropy. The change in entropy of the gas on both sides of the beam element can be expressed as the difference between two entropies caused by expansion $(h_1 + \Delta h_{ij})/h_1$ and compression $(h_1 - \Delta h_{ij})/h_1$.

$$\Delta S_{ij} = \Delta S_{ij}^E - \Delta S_{ij}^C = \frac{m \cdot R}{2 \cdot N \cdot M_m} \left(\ln \frac{h_1 + \Delta h_{ij}}{h_1} - \ln \frac{h_1 - \Delta h_{ij}}{h_1} \right) \approx \frac{m \cdot R}{N \cdot M_m} \cdot \frac{\Delta h_{ij}}{h_1}, \tag{15}$$

where displacement Δh_{ij} represents a small change in the piston height. It can be noted that the same formula can be derived by Shannon's entropy, which measures the information content in a given system [20]. The characteristic $\Delta h_{ij}/h_1$ can be interpreted as an analogy to strain ε in Hooke's laws. The small displacements are a standard condition in Euler–Bernoulli beam theory in structural mechanics. The magnitude of ΔS_{ij} can be expressed as:

$$\Delta S_{ij} \approx \frac{m \cdot R}{h_1 \cdot M_m} \cdot \frac{1}{N} \cdot \left| \Delta h_{ij} \right| = k_1 \cdot \frac{1}{N} \cdot \left| \Delta h_{ij} \right|, \text{ where } \Delta h_{ij} << h_1. \tag{16}$$

This equation expresses that there is an entropy change in the direction of deformation proportional to a constant and the displacement Δh_{ij}. The change in entropy is linearly dependent on displacement, similar to [93]. By substituting $\Delta h_{ij} = f_{ij}$ in Equation (5) into Equation (16), Equation (12) can be followed. In the following text, the change in entropy will be briefly referred to as entropy.

3.4. Entropy and Virtual temperature

In Equation (12), entropy and strain energy are additive quantities, so their values can be obtained by the summation of all elements. After introducing $\Delta h_{ij} = f_{ij}$, the summation of all j-th elements leads to:

$$\underbrace{i^4 \cdot E \cdot I \cdot \frac{c_i^2 \cdot \pi^4}{2 \cdot L^3} \cdot \frac{1}{N} \sum_{j=1}^{N} \left[\sin\left(i \frac{\pi \cdot (j - 0.5)}{N} \right) \right]^2}_{\Delta \Pi_i} = T_i \cdot \underbrace{k_1 \cdot \frac{1}{N} \cdot \sum_{j=1}^{N} \left| c_i \cdot \sin\left(i \frac{\pi \cdot (j - 0.5)}{N} \right) \right|}_{\Delta S_i}, \tag{17}$$

Preprints (www.preprints.org) | NOT PEER-REVIEWED | Posted: 14 November 2023 doi:10.20944/preprints202311.0862.v1

where $c_i>0$ is a scale factor of the i-th buckling mode. Equation (17) creates a connection between the products of the second derivative (bending moment) on the left-hand side and the product of deformation on the right-hand side. The sum of the absolute value of the sine function in Equation (17) converges to the value of $2 \cdot N/\pi$.

$$\lim_{N\to\infty} \sum_{j=1}^{N} \left| c_i \cdot \sin\left(i \frac{\pi \cdot (j-0.5)}{N} \right) \right| = 2 \cdot N \cdot \frac{c_i}{\pi}. \tag{18}$$

For $N > i$, Equation (18) takes the form of an approximate relationship. By substituting Equation (18) and Equation (9) into Equation (17), Equation (17) can be simplified to the form of Equation (19).

$$\underbrace{i^4 \cdot E \cdot I \cdot \frac{c_i^2 \cdot \pi^4}{4 \cdot L^3}}_{\Delta\Pi_i} = T_i \cdot \underbrace{2 \cdot k_1 \cdot \frac{c_i}{\pi}}_{\Delta S_i}, \tag{19}$$

where the left-hand side is the change in strain energy $\Delta\Pi_i$ and the right-hand side $T_i \cdot \Delta S_i$ takes into account the change in entropy. Due to the specific shape of the sine functions of the buckling modes, the entropy of the gas is a function of only the amplitude c_i and constant k_1.

$$\Delta S_i = 2 \cdot k_1 \cdot \frac{c_i}{\pi}, \tag{20}$$

where m is the mass of gas in all pistons and m, R, M_m, h_1 are constants. Equation (20) expresses the entropy of the gas in the surrogate model. The virtual temperature T_i of the gas calculated from the surrogate model of the pin-ended strut can be written using Equation (19) as:

$$T_i = i^4 \cdot c_i \cdot E \cdot I \cdot \frac{\pi^5}{8 \cdot k_1 \cdot L^3}. \tag{21}$$

The decomposition of $\Delta\Pi_i$ into T_i and ΔS_i introduced both T_i and ΔS_i as dependent on c_i, but only the virtual temperature T_i is a fourth power function of index i.

Equation (19) can be written using $P_{cr,i}$

$$\underbrace{\overbrace{\pi^2 \frac{E \cdot I}{L^2}}^{P_{cr,1}} \cdot i^4 \cdot \frac{c_i^2 \cdot \pi^2}{4 \cdot L}}_{\Delta\Pi_i} = \underbrace{\overbrace{\pi^2 \frac{E \cdot I}{L^2}}^{P_{cr,1}} \cdot i^4 \cdot \frac{c_i \cdot \pi^3}{8 \cdot k_1 \cdot L}}_{T_i} \cdot \underbrace{2 \cdot k_1 \cdot \frac{c_i}{\pi}}_{\Delta S_i}. \tag{22}$$

Equation (22) introduced the decomposition of strain energy $\Delta\Pi_i$ into terms of virtual temperature T_i and entropy ΔS_i. Changes in entropy exhibit linear dependence on displacement, analogous to [93]. The utilization of Equation (22) can be presented in two fundamental cases.

The case of constant entropy ΔS_i = constant: If we introduce $c_i = c_1$ as a constant for all buckling modes, then the strain energy increases with the fourth power of the index i, and entropy remains constant across all buckling modes. The first buckling mode, which has the lowest strain energy at constant entropy, is realized first.

The case of constant energy $\Delta\Pi_i$ = constant. If we introduce $c_i = c_1/i^2$, then the strain energy remains constant across all buckling modes, and entropy decreases with the square of index i. The first buckling mode, which has the highest entropy at constant energy, is realized first.

3.5. The Case study

Let us consider a pin-ended IPE240 steel beam with the length of L = 3m. The member has Young's modulus of E=210 GPa, and its second moment of area is $I = 2.83 \cdot 10^{-6}$ m^4. Euler's critical load is $P_{cr,1}$ = 651.7 kN. The results in Table 1 are obtained with the assumption of c_i = 1 m and k_1 = 1000 Jm^{-1}K^{-1}. Table 1 presents a scenario of constant entropy, as entropy does not depend on the buckling mode index.

Preprints (www.preprints.org) | NOT PEER-REVIEWED | Posted: 14 November 2023 doi:10.20944/preprints202311.0862.v1

Table 1. Ranking of buckling modes according to strain energy, assuming constant entropy.

Buckling mode index	Critical force $F_{rc,i}$ [kN]	c_i	Strain energy $\Delta\Pi_i$ [MJ]	Virtual temperature T_i [K]	Entropy ΔS_i [J·K^{-1}]
1	651.7	1	0.536	842.0	636.62
2	2606.9	1	8.576	13472.7	636.62
3	5865.5	1	43.418	68200.3	636.62
4	10427.6	1	137.221	215546.7	636.62
5	16293.1	1	335.013	526237.0	636.62
6	23462.0	1	694.683	1091205.0	636.62

In Equation (22), considering the decomposition of strain energy into entropy, virtual temperature is the measure by which energy is evaluated in terms of entropy.

The criterion that the equilibrium state can be characterized as a state of minimum energy for given entropy can be applied. The minimal strain energy occurs for the first buckling mode, which occurs first, see Table 1. Subsequent buckling modes are ranked in ascending order, just like according to critical forces. It holds that $\Delta\Pi_i = i^4 \cdot \Delta\Pi_1$.

The same conclusion can be obtained using the criterion that the equilibrium state can be characterized as a state of maximum entropy for a given energy. By using Equation (22), the amplitude (scale factor) needs to be set as decreasing across buckling modes $c_i = c_1/i^2$ in order to keep the strain energy constant across all modes. Using this new scale, the entropy of the buckling modes is computed, see the last column in the Table 2.

Table 2. Ranking of buckling modes according to entropy, assuming constant strain energy.

Buckling mode index	Critical force $F_{rc,i}$ [kN]	c_i	Strain energy $\Delta\Pi$i [MJ]	Virtual temperature T_i [K]	Entropy ΔS_i [J·K^{-1}]
1	651.7	1	0.536	1.0000	636.62
2	2606.9	0.25	0.536	15.3229	159.15
3	5865.5	0.111	0.536	25.0961	70.74
4	10427.6	0.063	0.536	58.2375	39.79
5	16293.1	0.04	0.536	72.6713	25.46
6	23462.0	0.028	0.536	130.7333	17.68

In Table 2, the criterion of maximum entropy for a given energy is applied. The first buckling mode, which occurs first, corresponds to the maximum entropy. Subsequent buckling modes are ranked in descending order, inversely to the ranking by critical forces.

The scale factor c_i in Table 2 decreases approximately as intensively as the mean values of the scale factors of the first three buckling modes for I-sections in [96]. The article [96] presents data in Table 1 from measurements of initial out-of-straightness from nine IPE 160 columns performed at the Polytechnic University of Milan and published by the ECCS 8.1 committee [97]. In addition, the article [96] uses the results from the measurements of 428 samples [98]. The scale factors c_i in Table 2 obtained from the analysis of strain energy and entropy are practically the same (differences are minimal) compared to the scale factors from experiments [96,97]. It is apparent that the scale factors c_i in Table 2 represent the measure of real initial imperfection. Thus, the initial imperfection can be introduced as a linear combination of the scaled buckling modes using their amplitudes $c_i = c_1/i^2$, where i is the index of the buckling mode and c_1 is the amplitude of the first buckling mode. The amplitudes c_i also express the (virtual) entropy for a given strain energy.

The ranking of buckling modes by strain energy in Table 1 and by entropy in Table 2 is the same. In the case study, both the criteria of minimum energy and maximum entropy lead to the same ranking of buckling modes.

Preprints (www.preprints.org) | NOT PEER-REVIEWED | Posted: 14 November 2023 doi:10.20944/preprints202311.0862.v1

4. Buckling of Cantilever

Let us assume that the entropy in Equation (16) can be applied to other patterns of buckling modes of other compression columns with different boundary conditions. The entropy of the i-th buckling mode can be obtained by summing the terms from Equation (16).

$$\Delta S_i = k_1 \cdot \frac{1}{N} \cdot \sum_{j=1}^{N} \left| \Delta h_{ij} \right|, \tag{23}$$

where k_1 is constant and h_{ij} is a deflection from the eigenvalue vector of the i-th buckling mode. Each eigenvector is dimensionless, with an indeterminate scale factor c_i. For example, the deformation of the i-th buckling mode of a cantilever can be expressed by the function:

$${}^{c}y(x) = c_i \cdot \left(1 - \cos\left((2i-1) \frac{\pi \cdot x}{2 \cdot L} \right) \right), \text{ for } \; x \in [0, L], \; i = 1, 2, .., \tag{24}$$

where $c_i > 0$. By substituting j/N for x/L, the continuous function can be written in the discrete form as:

$${}^{c}f_{ij} = c_i \cdot \left(1 - \cos\left((2i-1) \frac{\pi \cdot (j - 0.5)}{2 \cdot N} \right) \right), \text{ for } j = 0, 1, \ldots N. \tag{25}$$

For $\Delta h_{ij} = {}^{c}f_{ij}$, the entropy of the i-th buckling mode of the cantilever can be written as:

$${}^{c}\Delta S_i = k_1 \cdot \frac{1}{N} \cdot \sum_{j=1}^{N} \left| c_i \cdot \left(1 - \cos\left((2i-1) \frac{\pi \cdot (j - 0.5)}{2 \cdot N} \right) \right) \right|. \tag{26}$$

In contrast to a pin-ended strut, the entropy of cantilever buckling modes is not constant but slightly dependent on the i-th index, especially for the first buckling modes.

$${}^{c}\Delta S_i = k_1 \cdot c_i \cdot \left[1 + \frac{\cos(\pi \cdot i)}{\pi \cdot (i - 0.5)} \right], \tag{27}$$

where $[\cdot]$ is not constant across buckling modes. However, the change in entropy is small compared to the change in strain energy. The change in strain energy $\Delta\Pi_i$ of the i-th buckling mode of the cantilever can be derived analogously to the solution in Chapter 2.

$${}^{c}\Delta\Pi_i = \frac{1}{2} \cdot \int_0^L E \cdot I \left(\frac{dy^2(x)}{dx^2} \right)^2 dx = \frac{E \cdot I \cdot \pi^4 \cdot c_i^2}{64 \cdot L^3} \cdot (2 \cdot i - 1)^4 . \tag{28}$$

By substituting Equation (27) and Equation (28) into Equation (12), the virtual temperature ${}^{c}T_i$ can be written as:

$${}^{c}T_i = \frac{{}^{c}\Delta\Pi_i}{{}^{c}\Delta S_i} = (2 \cdot i - 1)^4 \cdot c_i \cdot \frac{E \cdot I \cdot \pi^4}{64 \cdot k_1 \cdot L^3} \cdot \left[\frac{\pi \cdot (i - 0.5)}{\pi \cdot (i - 0.5) + \cos(\pi \cdot i)} \right]. \tag{29}$$

If we introduce $c_i = c_2$ as a constant for all buckling modes, the strain energy greatly increases with the fourth power of index i. However, the entropy computed from the surrogate model changes slightly across the buckling modes.

5. Buckling of Steel Plane Frames

The design criteria for steel structures are built on the principles of natural sciences and empirical experience [2]. Engineers combine theoretical knowledge with practical expertise and innovations to design safe and reliable structures.

In the case of steel plane frames, it is typically assumed that the most critical mode is the first buckling mode with the lowest critical buckling load. This analysis suffices when the second critical load significantly exceeds the first critical load. However, if the first and second critical buckling loads coincide, it may be useful to explore alternative approaches for the ranking of buckling modes [18].

Preprints (www.preprints.org) | NOT PEER-REVIEWED | Posted: 14 November 2023 doi:10.20944/preprints202311.0862.v1

The change in strain energy for the i-th elastic buckling mode of the steel plane frame can be calculated using a second-order theory based finite element model (FEM); see, e.g., [19].

$$\Delta\Pi_i = \sum_{k=1}^{K}\left[\frac{1}{2}\cdot\int_0^{L_k} E\cdot I_k\left(\kappa_i\cdot\frac{dy_k^2(x)}{dx^2}\right)^2 dx\right], \tag{30}$$

where L_k is the length of the k-th member, I_k is the second moment of area of the k-th member, and $y_k(x)$ represents the deformation of the i-th elastic buckling mode of the k-th member. The input condition for addressing Equation (30) involves incorporating eigenmodes normalized to the sum of deformations equal to one.

A significant gap exists regarding the calculation of entropy change in buckled frames. Without consideration of entropy, strain energy is analysed with an undetermined scale, denoted as κ_i in Equation (30). It can be assumed that, for a given strain energy, the entropy will decrease analogously to the results in Table 2. The scale factor κ_i can be calibrated in such a way that the strain energy of each buckling mode is equal to the strain energy of the first mode. The most critical mode should have the highest entropy corresponding to the lowest critical force.

5.1. Steel Plane Frame: Case Study

The methodology for ranking buckling modes of steel plane frames can be illustrated in a case study. The columns and cross-beam of the frame are made of hot-rolled IPE240 members. The structural material is steel grade S235, with Young's modulus of elasticity E = 210 GPa, and the second moment of area for the IPE profile is I_y = 3890 cm^4. The geometry of the frame is shown in Figure 5

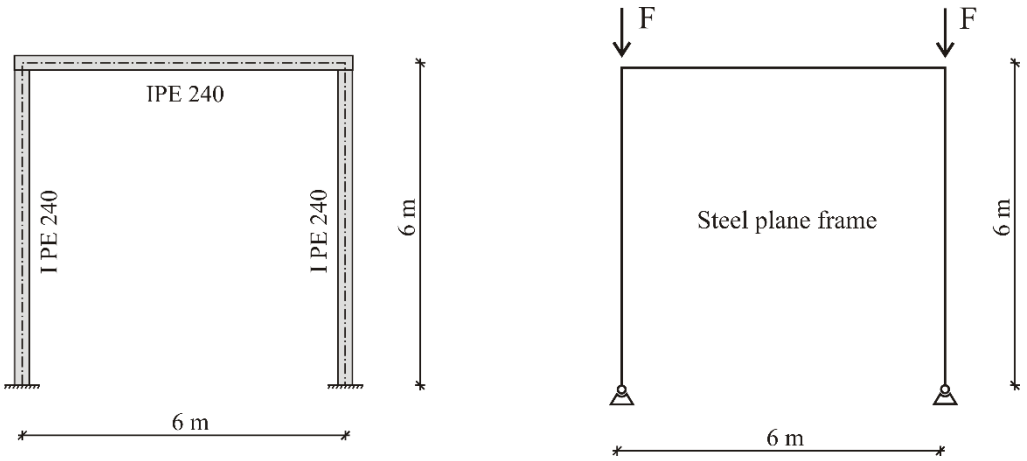

Figure 5. The geometry of the steel plane frame.

The frame is modelled using the finite element method, with stiffness matrices and geometric matrix of the beam finite element published in [19]. The frame is meshed using 37 nodes and 36 beam finite elements. Each element has 9 internal points where deformations are utilized. In total, there are 37 + 36*9 = 361 deformation points, where each point has one horizontal and one vertical deformation. The total deformation in each point, which has a general direction, is calculated using the Pythagorean theorem. Rotations are not considered. The vector of all 361 total deformations is normalized so that the sum of all total deformations equals one. The critical forces and corresponding buckling modes are computed using a second-order theory-based FEM [19], see Figure 6.

Preprints (www.preprints.org) | NOT PEER-REVIEWED | Posted: 14 November 2023 doi:10.20944/preprints202311.0862.v1

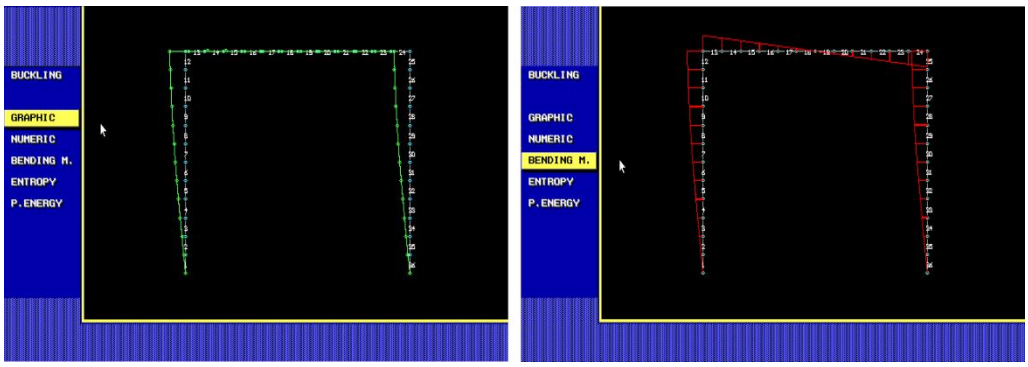

Figure 6. Second-order theory-based FEM: first buckling mode and bending moment.

The first six eigenvalues (critical forces) and eigenvector deformations (buckling modes) are computed using the step-by-step loading method, see Figure 7.

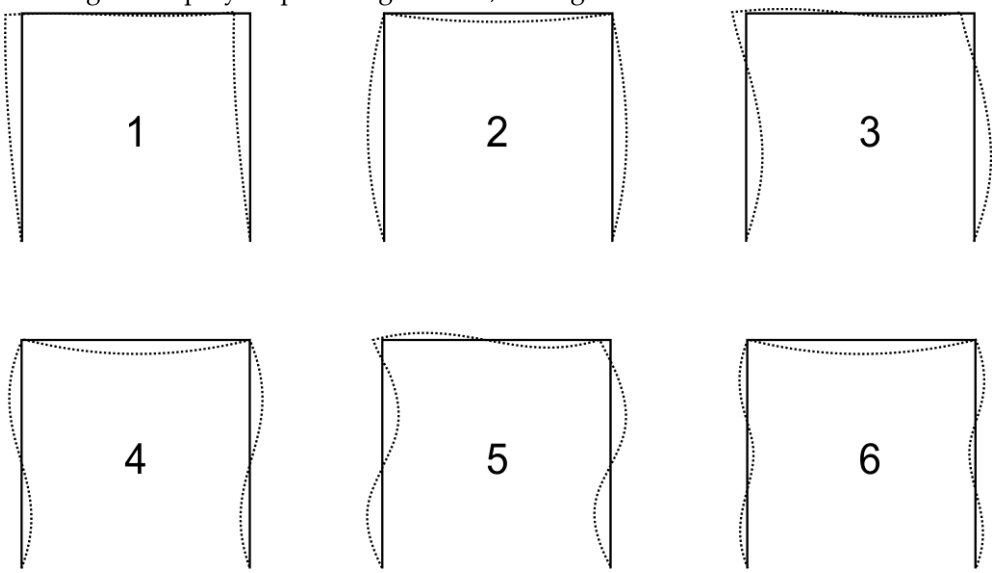

Figure 7. First six buckling modes of steel plane frame.

The procedure was practically carried out as follows: The critical forces $F_{cr,i}$ and the corresponding buckling modes (eigenvectors) were computed. Using κ_i =1 and the normalized scale of total deformations, the strain energies of the buckling modes were computed, see third column in Table 3. The strain energy from the third column approximately correlates with the strain energy calculated using the approximation formula $i^4\ \Delta\Pi_1$, where formula $i^4\ \Delta\Pi_1$ was explicitly derived for pin-ended struts.

Table 3. Ranking of the buckling modes according to the strain energy for given entropy.

Buckling mode index	Critical force $F_{rc,i}$ [kN]	Strain energy $\Delta\Pi i$ [J] (from normalized eigenmodes)	Scale factor κ_i (~ entropy)	Approximation of strain energy $\approx i^4\ \Delta\Pi_1$ [J]
1	412.5	1.1056	1.0000	1.1056
2	2925.8	61.3416	1.0000	17.6905
3	3830.9	101.8158	1.0000	89.5581
4	9784.0	451.7487	1.0000	283.0477
5	11085.0	880.4734	1.0000	691.0345
6	21023.4	1406.9822	1.0000	1432.9292

Preprints (www.preprints.org) | NOT PEER-REVIEWED | Posted: 14 November 2023 doi:10.20944/preprints202311.0862.v1

Equation (30) uses the scale factor κ_i, which influences $\Delta\Pi_i$. If the value κ_i =1, then $\Delta\Pi_i$ is solely computed from the normalized total deformations. The last column in Table 4 provides the approximation of entropy ~ κ_i, which sets the strain energy of the i-th buckling mode equal to the strain energy of the first buckling mode. The value of κ_i is calculated according to Equation (31).

$$\kappa_i = \sqrt{\frac{\Delta\Pi_1}{\Delta\Pi_i}}\,, \tag{31}$$

where strain energies under the square root are calculated solely from the normalized total deformations.

Table 4. Ranking of the buckling modes according to the entropy for given strain energy.

Buckling mode index	Critical force $F_{rc,i}$ [kN]	Given strain energy $\Delta\Pi_i$ [J] (by scaled eigenmodes)	Scale factor κ_i (for $\Delta\Pi_i = \Delta\Pi_1$)	Entropy ~ κ_i
1	412.5	1.1056	1.0000	1.0000
2	2925.8	1.1056	0.1343	0.1343
3	3830.9	1.1056	0.1042	0.1042
4	9784.0	1.1056	0.0495	0.0495
5	11085.0	1.1056	0.0354	0.0354
6	21023.4	1.1056	0.0180	0.0180

The strain energy can be roughly approximated as $\Delta\Pi_i \approx i^4\,\Delta\Pi_1$. Similarly, to the strain energy relationship between the frame and the pin-ended strut, a similar relationship for entropy can be assumed. Although the link is not direct, it can be expected that the change in entropy can be found to be linear in κ_i, albeit with the potential influence of additional factors. Although the equation for computing the frame's entropy has not been derived, a strong correlation between entropy (for a given energy) and results in the last column of Table 4 can be expected. The scale factor κ_i in the penultimate column can be heuristically considered as the entropy estimate, see Table 4.

If there is an estimate of entropy, the criterion that the equilibrium state can be characterized as a state of maximum entropy for a given energy can be applied. The maximum entropy occurs for the first buckling mode, which occurs first, see last column in Table 4. The same conclusion can be obtained using the criterion of minimum energy for the given entropy, see third column of Table 3.

6. Initial Geometrical Imperfections

The scaling of buckling modes can be used to create an initial imperfection to account for second-order geometrical nonlinearity. The classical method uses scaling the lowest eigenmode, see, e.g. [99,100]. The concept behind this theory is that the most critical imperfect geometry is the closest to the final collapse configuration since it requires the least deformation energy to go from the unloaded state to the final collapse situation [101].

Initial imperfections of frame structures can be based on scaled buckling modes. Such fitting of randomly generated shapes of imperfection have been introduced, e.g., in [102]. The method is based on the scale factors of cold-formed steel members calculated on the basis of experimental measurements [103]. Using the energy measure of eigenmodes to introduce initial imperfections has been presented for cold-formed steel columns [104] and axially compressed cylindrical shells [105]. In the case of shells, the energy measure of geometric imperfections was defined by the square root of the strain energy [104].

The introduction of initial frame imperfections using entropy as a supporting energy factor has not yet been presented. Entropy, as a complement to strain energy, plays an important role in structural stability analysis by justifying the scaling of buckling modes based on strain energy. The case study demonstrated rational scales of buckling modes with the dominant position of the first buckling mode. The ranking by strain energy is possible when the entropy remains constant across

Preprints (www.preprints.org) | NOT PEER-REVIEWED | Posted: 14 November 2023 doi:10.20944/preprints202311.0862.v1

all buckling modes, and analogously, ranking by entropy is achievable only under constant strain energy.

The scales of buckling modes exhibit a decreasing trend if the same strain energy is considered in each buckling mode, see Table 3. Such scaled buckling modes can be applied in the modelling of initial geometric imperfections. Examples of initial geometric imperfection shapes using combinations of scaled buckling modes are shown in Figure 8.

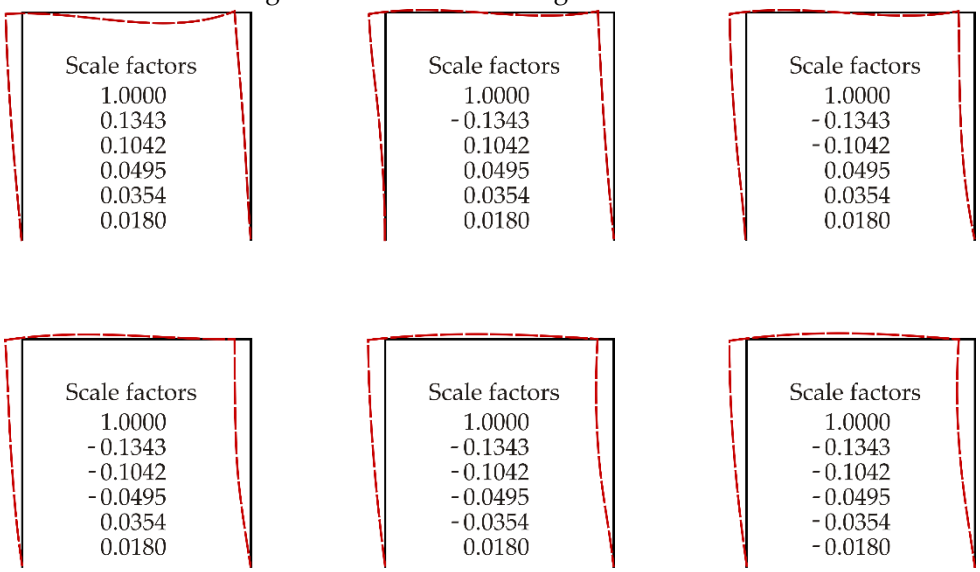

Figure 8. Initial imperfections from scaled buckling modes, first six combinations.

The signs of the scale factors of buckling modes create $2^6 = 64$ combinations. The first buckling mode is dominant and the other modes only slightly change its shape, see Figure 8. The basic assumption is that enough modes must be applied to ensure that deformations of critical elements are induced by imperfections [96]. However, the scale factors of higher-order modes decrease rapidly and their contribution can be neglected from a certain order. It can be noted that common engineering practice often uses only the first buckling mode [96]. To estimate the limit state, the initial imperfection should be close to the critical mode, which replaces the shape of the frame in the limit state with failure due to buckling. This approach is consistent with the EUROCODE 3 design standard [91].

In the stochastic approach, the initial imperfection can be thought of as an approximation of the real imperfection from measurements on a large number of frames. Scaled buckling modes can be used for the random simulation of the shapes of initial imperfections. One possibility is to consider the contributions of buckling modes with a mean value of zero (perfect strain frame) and random variability based on the scale factor. A similar approach has been applied in probabilistic reliability analyses [17,106].

7. Conclusions

The article investigated the duality of minimum energy and maximum entropy in the context of buckling. Entropy analysis of structures supports energy-based computational results and provides a rationale for ranking buckling modes based on strain energy. An explicit solution was derived for the relationship between strain energy and change in entropy within the context of the pin-ended strut. The change in entropy was found to be linear in displacement.

Entropy extends the applicability of the criterion of minimum energy in structural mechanics. Buckling modes can be ranked according to strain energy for the given entropy. Alternatively, buckling modes can be ranked according to entropy for the given strain energy. In both cases, the ranking aligns with the traditional method based on critical forces. For a given energy, scaled buckling modes coincide with experimentally determined initial imperfections of steel beams IPE160 [96,97].

In the case of frame structures, the scale factors of buckling modes demonstrate a decreasing trend when strain energy is constant in each mode. These scale factors can heuristically be interpreted as an estimate of entropy. Scaled buckling modes are valuable when dealing with initial geometric imperfections formed as their linear combination. Each buckling mode is assigned the same strain energy through a change in scale. The initial imperfection can be considered as a linear combination of these scaled buckling modes.

The case study illustrated rational scales with a dominant first buckling mode. The contribution of other modes diminishes as scale and entropy decrease. In future research, the initial imperfections can be further studied, opening up new possibilities for structural stability analysis.

Author Contributions: All aspects of this work, including software development, writing, and more, were solely undertaken by the single author.

Funding: The work has been supported and prepared within the project "Importance of Stochastic Interactions in Computational Models of Structural Mechanics" of The Czech Science Foundation (GACR, https://gacr.cz/) no. 23-04712S, Czechia.

Institutional Review Board Statement: Not applicable

Informed Consent Statement: Not applicable

Data Availability Statement: Not applicable

Conflicts of Interest: The author declares no conflict of interest

References

1. Bažant, Z.P.; Cedolin, L. *Stability of Structures: Elastic, Inelastic, Fracture and Damage Theories*; Oxford University Press, New York, 1991.
2. Galambos, T.V. *Guide to Stability Design Criteria for Metal Structures*, 5th ed.; Wiley: Hoboken, NJ, USA, 1998; 911p. [Google Scholar]
3. Godoy, L.A. Historical sense in the historians of the theory of elasticity. *Meccanica* **2006**, *41*, 529–538. [CrossRef]
4. Van Den Broek, J.A. Euler's classic paper "On the strength of columns". *Journal of Physics* **1947**, *12*, 309–318. [CrossRef]
5. Euler, L. *Methodus Inveniendi Lineas Curvas Maximi Minimive Proprietate Gaudentes, Sive Solutio Problematis Isoperimetrici Lattissimo Sensu Accepti*, Marcum Michaelem Bosquet, Lausanne, 1744.
6. Von Mises, R.; Ratzersdorfer, J. Die Knicksicherheit von Rahmentragwerken. *Zeitschrift für Angewandte Mathematik und Mechanik* (ZAMM) **1926**, 6, 181–199. [CrossRef]
7. Chwalla, E. Die Stabilität zentrisch und exzentrisch gedrückter Stäbe aus Baustahl, *Sitzungsberichte der Akademie der Wissenschaften mathematisch-naturwissenschaftliche Klasse* **1928**, *137*, 469–512.
8. Belytschko, T.; Liu, W.K.; Moran, B.; Elkhodary, K. *Nonlinear Finite Elements for Continua and Structures*, John Wiley & Sons, 2014.
9. Chan, S.L.; Huang, H.Y.; Fang, L.X. Advanced analysis of imperfect portal frames with semirigid base connections. *Journal of Engineering Mechanics* **2005**, 131, 633–640. [CrossRef]
10. Mageirou, G.E.; Lemonis, M.E. Influence of imperfections on the progressive collapse of steel moment resisting frames. *Journal of Constructional Steel Research* **2021**, *183*, 106744. [CrossRef]
11. Kala, Z.; Valeš, J. Sensitivity assessment and lateral-torsional buckling design of I-beams using solid finite elements. *Journal of Constructional Steel Research* **2017**, *139*, 110–122. [CrossRef]
12. Zhang, H. ; Shayan, S.; Rasmussen, K.J.R.; Ellingwood, B.R. System-based design of planar steel frames, I: Reliability framework. *Journal of Constructional Steel Research* **2016**, *123*, 135–143. [CrossRef]
13. Kala, Z.; Valeš, J.; Jönsson, J. Random fields of initial out of straightness leading to column buckling. *Journal of Civil Engineering and Management* **2017**, *23*, 902–913. [CrossRef]
14. Jindra, D.; Kala, Z.; Kala, J. Buckling curves of stainless steel CHS members: Current state and proposed provisions. *Journal of Constructional Steel Research* **2022**, *198*, 107521. [CrossRef]
15. Jindra, D.; Kala, Z.; Kala, J. Flexural buckling of stainless steel CHS columns: Reliability analysis utilizing FEM simulations. *Journal of Constructional Steel Research* **2022**, *188*, 107002. [CrossRef]
16. Gu, J.X.; Chan, S.L. Second-order analysis and design of steel structures allowing for member and frame imperfections. *International Journal for Numerical Methods in Engineering* **2005**, *62*, 601–615. [CrossRef]
17. Kala, Z. Global sensitivity analysis in stability problems of steel frame structures. *Journal of Civil Engineering and Management* **2016**, *22*, 417–424. [CrossRef]

18. Bažant, Z.; Xiang, Y. Postcritical imperfection-sensitive buckling and optimal bracing of large regular frames. *Journal of Structural Engineering* **1997**, *123*, 513–522. [CrossRef]
19. Kala, Z. Geometrically non-linear finite element reliability analysis of steel plane frames with initial imperfections. *Journal of Civil Engineering and Management* **2012**, *18*, 81–90. [CrossRef]
20. Ben–Naim, A. *A Farewell to Entropy: Statistical Thermodynamics Based on Information;* World Scientific, Singapore, 2008.
21. Charlton, T.M. *Energy Principles in Theory of Structures*; Oxford University Press, 1973.
22. Arthurs, A.M.; Jones, M.E. On variational principles for linear initial value problems. *Journal of Mathematical Analysis and Applications* **1976**, *54*, 840–845. [CrossRef]
23. Van Groesen, E.W.C. *Variational Methods in Mathematical Physics;* Technische Hogeschool Eindhoven, 1978, p.216. [CrossRef]
24. Washizu, K. *Variational Methods in Elasticity and Plasticity;* Pergamon Press: Oxford, UK, 1982; p.630.
25. Auchmuty, G. Duality for non-convex variational principles. *Journal of Differential Equations* **1983**, *50*, 80–145. [CrossRef]
26. Berdichevsky, V.L. *Variational Principles of Continuum Mechanics*; Springer: Berlin/Heidelberg, Germany, 2009, p.1011.
27. Fanaie, N.; Shirpour, A. Analytical and numerical evaluation of quarter-elliptic-braced steel moment frames (QEB-MFs). *Structures* **2023**, *49*, 426–442. [CrossRef]
28. Zheng, A.; Shi, H.-R.; Gong, Z.; Wang, C.-L.; Meng S. Experimental study on bamboo-shaped buckling-retrained energy dissipater with different grades of steel. *Journal of Constructional Steel Research* **2023**, *211*, 108164. [CrossRef]
29. Ou, T.; Mei, C.; Mao, J.; Wang, D. Seismic analysis and connection optimization of the side column on modular prefabricated four-sided connected composite shear wall. *The Structural Design of Tall and Special Buildings* **2022**, *32*, 426–442. [CrossRef]
30. Gorgogianni, A.; Eliáš, J.; Le, J.-L. Mesh objective stochastic simulations of quasibrittle fracture. *Journal of the Mechanics and Physics of Solids* **2022**, *159*, 104745. [CrossRef]
31. Zheng, X.; Shen, Y.; Zong, X.; Su, H.; Zhao, X. Vulnerability analysis of main aftershock sequence of aqueduct based on incremental dynamic analysis method. *Buildings* **2023**, *13*, 1490. [CrossRef]
32. Yang, J.; Wang, W.; Xu, L.; Shi, Y. Global buckling analysis on cold-formed steel built-up box-shape columns at ambient and elevated temperatures. *Structures* **2023**, *57*, 105301. [CrossRef]
33. Hamed, A.A.; Samadi, A.; Charkhtab Basim, M. Topology and shape optimization of steel plate shear walls for enhancing the seismic energy dissipation capacity. *Journal of Building Engineering* **2022**, *57*, 104828. [CrossRef]
34. Zheng, Z.-Q.; Liu, H.-Z.; Zhuo, L.; Xiao, M.-L.; Xie, H.-Q.; He, J.-D.; Peng, M.-L. Experimental study on the dilatancy and energy evolution behaviors of red-bed rocks under unloading conditions. *Materials* **2023**, *16*, 5759. [CrossRef]
35. Lu, H.; Pan, Y.; He, K.; Wang, F.; Gao, L.; Pu, S.; Li, E. Dynamic Mechanical Properties and Damage Evolution Characteristics of Beishan Deep Granite under Medium and High Strain Rates. *Materials* **2023**, *16*, 5235. [CrossRef]
36. Fujii, K. Peak and Cumulative Response of Reinforced Concrete Frames with Steel Damper Columns under Seismic Sequences. *Buildings* **2022**, *12*, 275. [CrossRef]
37. Pandit, U.K.; Mondal, G.; Punera, D. Lateral torsional buckling analysis of corrugated steel web girders using homogenization approach. *Journal of Constructional Steel Research* **2023**, *210*, 108099. [CrossRef]
38. Rezaiee-Pajand, M.; Masoodi, A.R.; Alepaighambar, A. Critical buckling moment of functionally graded tapered mono-symmetric I-beam. *Steel and Composite Structures* **2021**, *39*, 599–614. [CrossRef]
39. Stupishin, L.; Mondrus, V. Implementation of the weak link problem for trusses. *Buildings* **2023**, *13*, 1230. [CrossRef]
40. Dehwah, O.H.A.; Al-Gahtani, H.J. Energy-based solution for the plastic buckling of stainless steel circular cylindrical shells. *Structures* **2023**, *48*, 2024–2036. [CrossRef]
41. Jafari, M.M.; Jahandari, S.; Ozbakkaloglu, T.; Rasekh, H.; Jahed Armaghani, D.; Rahmani, A. Mechanical properties of polyamide fiber-reinforced lime–cement concrete. *Sustainability* **2023**, *15*, 11484. [CrossRef]
42. Fujii, K.; Mogi, Y.; Noguchi, T. Predicting maximum and cumulative response of a base-isolated building using pushover analysis. *Buildings* **2020**, *10*, 91. [CrossRef]
43. Muc, A. Buckling of composite structures with delaminations—laminates and functionally graded materials. *Appl. Sci.* **2022**, *12*, 11408. [CrossRef]
44. Shima, H. Buckling of carbon nanotubes: A state of the art review. *Materials* **2012**, *5*, 47-84. [CrossRef]
45. Chen, L.; Yao, X.; Sun, Z. Wang, D. Study seismic performance of duplex stainless steel under large strain amplitude by cyclic loading test. *Journal of Constructional Steel Research* **2022**, *194*, 107332. [CrossRef]
46. Liu, C.; Sun, Z. Calculation theory of shear stress distribution in box girder with corrugated steel webs based on the energy method. *Buildings* **2023**, *13*, 2547. [CrossRef]

47. Khaleel Ibrahim, S.; Movahedi Rad, M. Optimal elasto-plastic analysis of prestressed concrete beams by applying residual plastic deformation limitations. *Sustainability* **2023**, *15*, 5742. [CrossRef]
48. Xiao, X.; Zhang, Q.; Zheng, J.; Li, Z. Analytical model for the nonlinear buckling responses of the confined polyhedral FGP-GPLs lining subjected to crown point loading. *Engineering Structures* **2023**, *282*, 115780. [CrossRef]
49. Hai, L.; Ban, H.; Yang, X.; Huang, C.; Shi, Y. Cyclic behavior of hot-rolled titanium-clad bimetallic steel under large plastic strain reversals. *Journal of Constructional Steel Research* **2023**, *210*, 108112. [CrossRef]
50. Stupishin, L.; Mondrus, V. Critical Energy Properties Study for Unsymmetrical Deformable Structures. *Buildings* **2022**, *12*, 779. [CrossRef]
51. Kala, Z.; Kalina, M. Static equilibrium states of von Mises trusses. *International Journal of Mechanics* **2016**, 2016, *10*, s. 294–298.
52. Chen, L.-M.; Li, Z.-B.; Zhang, H.; Liu, Y.-J.; Zeng, Y.-H.; Zhou, Y.-Y.; Dong, S.-L. Design optimisation of a cable–strut tensile structure according to the importance of elements. *Buildings* **2022**, *12*, 1528. [CrossRef]
53. Simão, P.D.; Rodrigues, J.P.C.; Fernandes, H.D. A voxels-based Rayleigh-Ritz method for the post-buckling elasto-plastic analysis of restrained steel columns in fire. *Journal of Constructional Steel Research* **2023**, *210*, 107736. [CrossRef]
54. Abdelrahman, A.H.A.; Lotfy, S.; Liu, S.-W. Generalized line-element formulations for geometrically nonlinear analysis of nonsymmetric tapered steel members with warping and Wagner effects. *Engineering Structures* **2022**, *273*, 115052. [CrossRef]
55. Kerdsuk, P.; Pulngern, T.; Tangbanjongkij, C.; Chucheepsakul, S.; Jiammeepreecha, W. Elastic buckling of oblate hemi-ellipsoidal shells subjected to hydrostatic pressure. *International Journal of Structural Stability and Dynamics*, **2023**, *2023*, 2450028. [CrossRef]
56. Elsayed, M.; A. Mutalib, A.; Elsayed, K. Numerical study of structural performance and wind flow dynamic behavior for PPVC steel modular construction (MSC) under various extreme wind loads. *Buildings* **2022**, *12*, 1347. [CrossRef]
57. Hajdú, G.; Pasternak, H.; Papp, F. Lateral-torsional buckling assessment of I-beams with sinusoidally corrugated web. *Journal of Constructional Steel Research* **2023**, *207*, 107916. [CrossRef]
58. Li, C.; Liu, N.; Liu, W.; Feng, R. Study on characteristics of energy storage and acoustic emission of rock under different moisture content. *Sustainability* **2021**, *13*, 1041. [CrossRef]
59. Zhang, X.; Sun, Y.; Yang, X.; Sun, L.; Wang, P. Study on the bending performance of high-strength and high-ductility CRE-reinforced concrete beams. *Buildings* **2023**, *13*, 2746. [CrossRef]
60. Godoy, L.A.; Ameijeiras, M.P. Plastic buckling of oil storage tanks under blast loads. *Structures* **2023**, *53*, 361–372. [CrossRef]
61. Luo, L.; Zhang, Y. A new method for establishing the total potential energy equations of steel members based on the principle of virtual work. *Structures* **2023**, *52*, 904–920. [CrossRef]
62. Zhang, Y.; Zhong, L.; Pang, F.; Li, P.; Liu, F. Characteristics of energy dissipation in T-Shaped fractured rocks under different loading rates. *Sustainability* **2023**, *15*, 13695. [CrossRef]
63. Sun, G.; Lai, J.; Zheng, Y.; Zheng, K.; Shi, J. Investigation of the performance of RC beams reinforced with FRP and ECC materials. *Journal of Civil Engineering and Management* **2022**, *28*, 523–535. [CrossRef]
64. Clausius, R. Ueber verschiedene für die Anwendung bequeme Formen der Hauptgleichungen der mechanischen Wärmetheorie. *Annalen der Physik* **1865**, 201, 353–400. (In German) [CrossRef]
65. Wang, X.; Qian, L.; Hong, M.; Zhang, J. Evolution and abrupt change for water use structure through matrix-based Renyi's alpha order entropy functional. *Stochastic Environmental Research and Risk Assessment* **2022**, *36*, 1413–1428. [CrossRef]
66. Jessop, A. Some reflections on maxEnt. *Civil Engineering and Environmental Systems* **2023**, *40*, 60–71. [CrossRef]
67. Chen, C.; Yang, Y.; Hou, H.; Peng, C.; Xu, W. Real-time hybrid simulation with multi-fidelity Co-Kriging for global response prediction under structural uncertainties. *Earthquake Engineering and Structural Dynamics* **2022**, 51, 2591–2609. [CrossRef]
68. Gao, C.; Elzarka, H.; Yan, H.; Chakraborty, D.; Zhou, C. A hybrid TOPSIS-structure entropy weight group subcontractor selection model for large construction companies. *Buildings* **2023**, *13*, 1535. [CrossRef]
69. Wang, Y.; Sun, Q.; Leng, S.; Cui, H.; Xu, B. Effect of dry-wet cycles on mechanical properties of polyurethane porous mixture. *International Journal of Pavement Engineering* **2023**, *24*, 2212315. [CrossRef]
70. Qiu, D.; Chen, J.; Fu, H. Research on the comprehensive evaluating index of seismic performance of underground large-scale frame structures. *Structures* **2022**, 37, 645–660. [CrossRef]
71. Pedretti, D.; Bianchi, M. GEOENT: A toolbox for calculating directional geological entropy. *Geosciences* **2022**, *12*, 206. [CrossRef]
72. Keerthana, M.; Harikrishna, P. Signal complexity approach based investigation of flutter instability in sectional models of bridges in wind tunnel. *Advances in Structural Engineering* **2023**, *26*, 2520–2542. [CrossRef]

73. Wang, Y.; Qu, Z. TMD Design by an Entropy Index for Seismic Control of Tall Shear-Bending Buildings. *Entropy* **2023**, *25*, 1110. [CrossRef]
74. Abi, E.; Yuan, H.; Cong, Y.; Wang, Z.; Jiang, M. Experimental study on the entropy change failure precursors of marble under different stress paths. *KSCE Journal of Civil Engineering* **2023**, *27*, 356–370. [CrossRef]
75. Luo, D.; Dong, H.; Niu, D. Geographic division of exposure environment for concrete structure based on fuzzy clustering-rough set information entropy. *Structural Concrete* **2023**, *24*, 485–503. [CrossRef]
76. Wang, C.; Zou, F.; Yap, J.B.H.; Wood, L.C.; Li, H.; Ding, L. System dynamics tool for entropy-based risk control on sleeve grouting in prefabricated buildings. *Engineering, Construction and Architectural Management* **2023**, *30*, 538–567. [CrossRef]
77. Su, L.; Wang, T.; Li, H.; Chao, Y.; Wang, L. Multi-criteria decision making for identification of unbalanced bidding. *Journal of Civil Engineering and Management* **2020**, *26*, 43–52. [CrossRef]
78. Xie, W.; Gao, D.; Lee, E.W. Detecting undeclared-leader-follower structure in pedestrian evacuation using transfer entropy. *IEEE Transactions on Intelligent Transportation Systems* **2022**, *23*, 17644–17653. [CrossRef]
79. Yang, N.; Jia, Y.T.; Bai, F.; Qin, S.J. Reliability estimation of a Tibetan heritage timber structure with inclination in its Que-Ti joints. *Structures* **2022**, *43*, 257–270. [CrossRef]
80. Luo, Z.; Guo, J.; Han, J.; Wang, Y. Reliability estimation of a Tibetan heritage timber structure with inclination in its Que-Ti joints. *Engineering, Construction and Architectural Management* **2022**. [CrossRef]
81. Kamiński, M.; Strąkowski, M. An application of relative entropy in structural safety analysis of elastoplastic beam under fire conditions. *Energies* **2023**, *16*, 207. [CrossRef]
82. Wang, T.; Li, Z.; Fan, W.; Ang, A.H.-S. Structural system reliability assessment using generalized factorized dimensional reduction method and iterative maximum entropy method. *Structure and Infrastructure Engineering* **2022**. [CrossRef]
83. Civera, M.; Surace, C. Instantaneous spectral entropy: An application for the online monitoring of multi-storey frame structures. *Buildings* **2022**, *12*, 310. [CrossRef]
84. Qu, S.; Fang, Y.; Liang, J.; Zheng, J.-H.; Zheng, K. A Physical mechanism-based model of CoCrFeMnNi high entropy alloy considering adiabatic heat effect for hot bulk forming processes. *Metals* **2022**, *12*, 1011. [CrossRef]
85. Shi, J.; Gong, H.; Yang, F.; Liang, H.; Cong, L. Image processing of aggregate skeleton structure of asphalt mixture for aggregate uniformity quantification. *Journal of Materials in Civil Engineering* **2023**, *35*, 04022388. [CrossRef]
86. Krylovas, A.; Kosareva, N.; Zavadskas, E.K. WEBIRA-Comparative analysis of weight balancing method. *International Journal of Computers, Communications and Control* **2017**, *12*, 238–253. [CrossRef]
87. Kala, Z. New importance measures based on failure probability in global sensitivity analysis of reliability. *Mathematics* **2021**, *9*, 2425. [CrossRef]
88. Kala, Z. Modelling initial geometric imperfections of steel plane frames using entropy and eigenmodes. *International Journal of Mechanics* **2023**, *17*, 64–73. [CrossRef]
89. Callen, H.B. *Thermodynamics and an Introduction to Thermostatistics*, John Wiley & Sons, 1985.
90. Yang, B. *Stress, Strain, and Structural Dynamics*, Elsevier Inc., 2005 [CrossRef]
91. European Committee for Standardization (CEN). EN 1993-1-9. *Eurocode3: Design of Steel Structures, Part 1–1: General Rules and Rules for Buildings*; European Standards: Brussels, Belgium, 2005. [CrossRef]
92. Feistel, R.; Ebeling, W. Entropy and the self-organization of information and value. *Entropy* **2016**, *18*, 193. [CrossRef]
93. Verlinde, E. On the origin of gravity and the laws of Newton. *Journal of High Energy Physics* **2011**, 2011, 29. [CrossRef]
94. Klotz, I.M.; Rosenberg, R.M. *Chemical Thermodynamics: Basic Concepts and Methods*, John Wiley & Sons, 2008.
95. Atkins, P.W. *Physical Chemistry*, New York: Freeman, 1998. [CrossRef]
96. Liu, W.; Rasmussen, K.J.R.; Zhang, H.; Xie, Y.; Liu, Q., Dai, L. Probabilistic study and numerical modelling of initial geometric imperfections for 3D steel frames in advanced structural analysis. *Structures* **2023**, *57*, 105190. [CrossRef]
97. Sfintesco, D. Fondement expérimental des courbes européennes de flambement, *Construction Métallique* **1970**, 3, 5–12.
98. Fukumoto, Y.; Itoh, Y. Evaluation of multiple column curves using the experimental data-base approach. *Journal of Constructional Steel Research* **1983**, *3*, 2–19. [CrossRef]
99. Gu, J.X.; Chan, S.L. Second-order analysis and design of steel structures allowing for member and frame imperfections. *International Journal for Numerical Methods in Engineering* **2005**, *62*, 601–615. [CrossRef]
100. Kim, S.-E.; Lee, D.-H. Second-order distributed plasticity analysis of space steel frames. *Engineering Structures* **2002**, *24*, 735–744. [CrossRef]
101. Alvarenga, A.R.; Silveira, R.A.M. Second-order plastic-zone analysis of steel frames - Part II: Effects of initial geometric imperfection and residual stress. *Latin American Journal of Solids and Structures* **2009**, 6, 323–342. [CrossRef]

102. Shayan, S.; Rasmussen, K.J.R.; Zhang, H. On the modelling of initial geometric imperfections of steel frames in advanced analysis. *Journal of Constructional Steel Research* **2014**, *98*, 167–177. [CrossRef]
103. Zeinoddini, V.M.; Schafer, B.W. Simulation of geometric imperfections in cold-formed steel members using spectral representation approach. *Thin-Walled Structures* **2012**, *60*, 105–117. [CrossRef]
104. Sadovský, Z.; Kriváček, J.; Ivančo, V.; Ďuricová, A. Computational modelling of geometric imperfections and buckling strength of cold-formed steel. *Journal of Constructional Steel Research* **2012**, *78*, 1–7. [CrossRef]
105. Sadovský, Z.; Kriváček, J. Influential geometric imperfections in buckling of axially compressed cylindrical shells – A novel approach. *Engineering Structures* **2020**, *223*, 111170. [CrossRef]
106. Kala, Z. Sensitivity analysis of steel plane frames with initial imperfections. *Engineering Structures* **2011**, *33*, 2342–2349. [CrossRef]